Chemical Science

Accepted Manuscript

This article can be cited before page numbers have been issued, to do this please use: S. Singh, G. Sharma, M. Joshi and V. Polshettiwar, *Chem. Sci.*, 2026, DOI: 10.1039/D5SC08424E.

ROYAL SOCIETY OF CHEMISTRY

rsc.li/chemical-science

Solar-Driven Upcycling of Plastic Waste Using Plasmonic Black Gold

Saideep Singh,# Gunjan Sharma,# Mamata Joshi, and Vivek Polshettiwar*

Department of Chemical Sciences, Tata Institute of Fundamental Research, Mumbai, 40005 India.

Email: vivekpol@tifr.res.in , # shared 1st authors

View Article Online
DOI: 10.1039/D5SC08424E

Abstract: Plastic waste accumulation poses a pressing environmental challenge, calling for sustainable routes to convert it into value-added products under mild conditions. Conventional Lewis acid-mediated upcycling relies on hydride transfer and carbocation formation but requires ionic liquids to stabilize intermediates and sacrificial alkylating agents like isopentane to overcome thermodynamic barriers. Here, we present a solar-driven, sacrificial-agent-free approach for catalytic plastic upcycling using plasmonic black gold nanostructures. Under visible-to-NIR irradiation, black gold activates tert-butyl chloride (TBC) through combined photothermal and hot-electron driven activation, generating reactive carbocations in polymer chains while converting Al_2Cl_6 into catalytically active $AlCl_3$ *in-situ*. This dual activation eliminates the need for ionic liquids and isopentane, enhancing both efficiency and sustainability. The system achieves >80% plastic conversion within one hour solely by light illumination with >85% selectivity toward branched C_6-C_{10} alkanes. Mechanistic studies confirm that plasmonic excitation promotes TBC dissociation and sustains $AlCl_3$ generation throughout the catalytic cycle. The catalyst exhibits excellent recyclability over multiple cycles without loss of activity or selectivity. A proof-of-concept outdoor experiment under natural sunlight further validates its real-world applicability. This work represents unique demonstration of plastic upcycling powered solely by sunlight using a plasmonic catalyst, merging broadband light harvesting, hot-carrier chemistry, and Lewis acid catalysis into a unified, sustainable platform for decentralised upcycling of plastic waste.

Keywords: Plasmonic catalysis, Plastic upcycling, Black gold nanoparticles, Hot electrons, Solar-driven chemical transformation

INTRODUCTION

The global accumulation of plastic waste poses a growing environmental and resource challenge. These polymers are chemically inert, thermally stable, and widely used, making their recycling particularly difficult.[1-4] Traditional recycling methods (mechanical reprocessing, pyrolysis, etc.) often suffer from high energy use, limited product value, and downcycling of material properties. On the other hand, chemical upcycling offers a pathway to transform waste plastics into valuable fuels and fine chemicals. However, current catalytic upcycling strategies often require harsh conditions, including high temperatures, pressurised hydrogen, reactive solvents, or complex co-reactants, limiting their environmental and economic viability.[1-7]

A notable breakthrough was recently reported,[8,9] where the authors introduced a tandem catalytic system using a Lewis acidic ionic liquid in iso-pentane (iC$_5$) to convert polyolefins into liquid alkanes at ~70 °C. Their system cleverly couples C-C bond cleavage with *in-situ* alkylation, enabling efficient low-temperature upcycling. However, despite its ingenuity, the method still depends on (i) external thermal input, (ii) specific hydrocarbon co-reactants (iC$_5$), and (iii) ionic liquids, which are expensive, corrosive, and difficult to scale.

Photocatalytic upcycling of plastic waste has emerged as a promising strategy to upcycle polymers under mild conditions using solar energy.[10-14] A variety of innovative photocatalytic systems have been reported for the upcycling of plastic waste, reflecting remarkable progress in this emerging field. Semiconductors such as MoS_2/g-C_3N_4 heterojunctions,[15] CN_x|Ni_2P,[16] ultrathin Nb_2O_5 layers,[17] and vanadium-based oxides[18] have demonstrated efficient charge separation and light harvesting. Organic photocatalysts, including $BrCH_2CN$-thioxanthone,[19] anthraquinone,[20] and phenothiazine derivatives,[21] have offered elegant metal-free strategies, while hybrid and composite systems, such as CdS/CdO_x quantum dots,[22] sulfur-vacancy-rich CdS,[23] Co-Ga_2O_3,[24] Zr-doped $CoFe_2O_4$ quantum dots[25] and iridium complexes,[26] have shown excellent activity and selectivity. Furthermore, enzyme-assisted platforms like TiO_2|CotpyP [27] and single-atom catalysts like M_1-TiO_2[28] highlight the diversity of mechanistic approaches being pursued. Acid-mediated photocatalysis using $AlCl_3$[29] or pTsOH[30] as well as $FeCl_3$[31] have provided compelling routes to oxygenates and monomers under mild conditions. Photothermal catalysis employing systems like Ni-TiO_2-Al_2O_3,[32] Ru-TiO_2,[33] TiO_2-DEG,[34] carbon quantum dots,[35] Cu/2D silicon in ionic liquid [36] provides a complementary route for plastic upcycling, where light energy is harnessed to generate localized heating and promote bond cleavage.

Despite these significant achievements, many of these systems rely on additives such as sacrificial electron

donors, alkylating agents, expensive solvents, ionic liquids or hydrogen gas. Others require elevated temperatures or UV light, which can limit sustainability and scalability. Thus, while the current body of work has laid a strong foundation, there remains a need for photocatalytic strategies that enable selective alkane generation from plastics using only solar light, without external heating, sacrificial reagents, or expensive solvents such as ionic liquids.

In this context, we pursued a distinct strategy, in favour of a purely sunlight-driven approach enabled by localised surface plasmon resonance (LSPR)-mediated photocatalysis.[37-48] Building on our prior work in designing plasmonic nanocatalysts with strong light-harvesting and catalytic capabilities,[49-57] we here report the upcycling of polyolefin plastic waste without external heating using plasmonic black gold[51-54] and $AlCl_3$ Lewis acid sites. *"Black Gold"* consists of uniformly distributed gold (Au) nanoparticles on dendritic fibrous nanosilica (DFNS) and exhibits broadband localised surface plasmon resonance (LSPR), enabling efficient harvesting of solar energy from the visible to near-infrared (NIR) region.[51-54] It generates energetic hot electrons that aid the formation of $AlCl_3$ from Al_2Cl_6, facilitate carbenium ion formation and sequential C-C bond scission in polyolefins. The system operates without ionic liquids, without any sacrificial hydrocarbons like iC_5, or any external thermal energy input. It facilitates the selective production of hydrocarbons and fine chemicals from waste plastics. Mechanistic studies support significant contribution of non-thermal activation pathway along with photothermal effects, wherein plasmon-induced hot electrons promote Lewis acid site-mediated cracking of polyolefins with high efficiency.

RESULTS AND DISCUSSION

Synthesis and Characterization of Broadband Black Gold Nanostructures. Dendritic plasmonic colloidosomes (DPC), also referred to as black gold, was synthesized following our previously reported one-pot protocol.[52] Comprehensive structural and compositional analyses were conducted to evaluate their morphology and plasmonic architecture (Fig. 1). Scanning electron microscopy (SEM) and transmission electron microscopy (TEM) (Fig. 1a) show fibrous nanosilica spheres (~400 nm) of DFNS uniformly loaded with gold nanoparticles (Au NPs), with an average particle size of ~8.6 nm (Fig. 1f). Energy-dispersive X-ray spectroscopy (EDS) mapping confirmed a uniform gold loading (48 wt.%), homogeneously distributed across the dendritic silica support (Fig. 1b-e, Table S1).

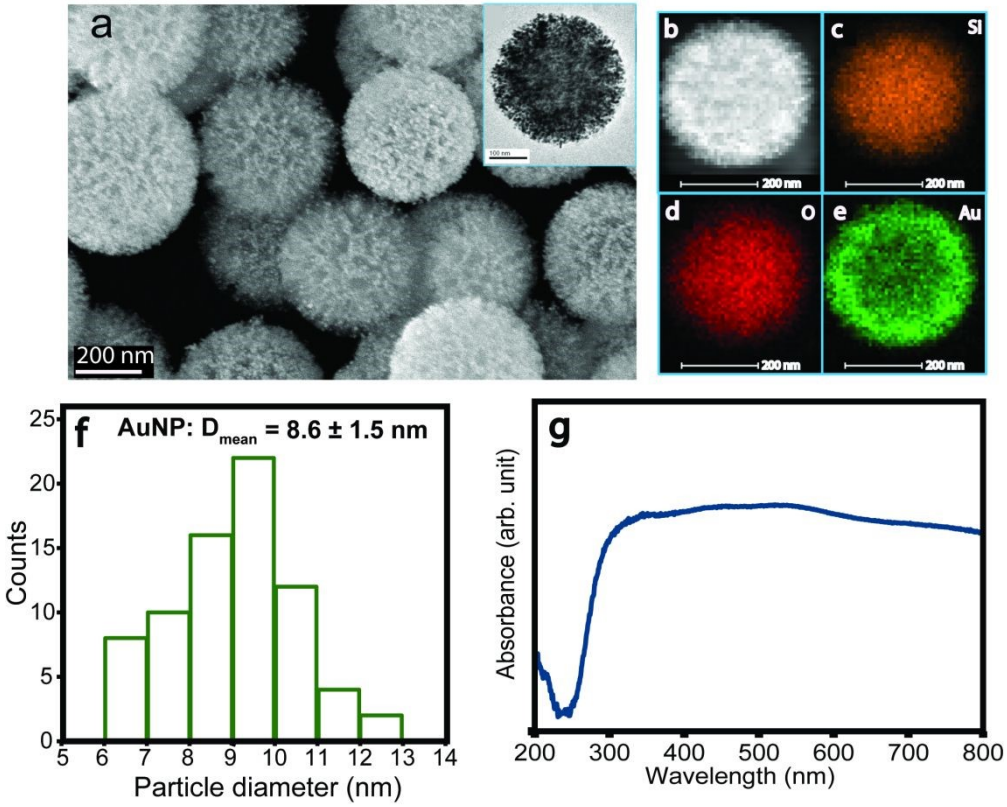

Fig. 1. Characterization of dendritic plasmonic colloidosomes (Black gold). (a) SEM images of DPC, inset: TEM image of DPC; **(b-e)** HAADF-STEM image of DPC and the corresponding elemental mapping; **(f)** Particle size distribution of Au nanoparticles in DPC and **(g)** UV-Vis diffuse reflectance spectra of DPC showing broadband absorption.

View Article Online DOI: 10.1039/D5SC08424E

X-ray diffraction (XRD) verified the formation of metallic Au phases (Fig. S1). Nitrogen sorption analysis indicated a high surface area (192 $m^2 g^{-1}$) and a pore volume of 0.23 $cm^3 g^{-1}$ (Fig. S2). The synthesis process involved controlled nucleation and growth of Au NPs on high-surface-area dendritic fibrous nanosilica, yielding a heterogeneous distribution of interparticle distances and particle sizes. This variability enables black gold to achieve broad-spectrum light absorption, spanning the visible to near-infrared (NIR) range (Fig. 1g) by virtue of the plasmonic coupling. The coexistence of diverse particle sizes and plasmonic coupling among Au NPs induces localized electric field hotspots, which can potentially enhance their catalytic efficiency during waste plastic upcycling.

Plasmonic Upcycling of Polyolefins. To study a solar-driven plasmonic upcycling of waste plastic, the photocatalytic reactions were conducted in a glass reactor under simulated solar illumination using a xenon lamp (400-1600 nm, 1.6 W cm^{-2}, Fig. S3). The catalytic process consisted of black gold as a plasmonic light harvester, tert-butyl chloride (TBC) as a source of tertiary carbenium ions to initiate the chain reaction, and Al_2Cl_6 as a precursor for generating $AlCl_3$ Lewis acid sites that facilitate hydride transfer. Due to photothermal and non-thermal effects (electric field enhancement and hot electron injection), plasmonic black gold was hypothesised to activate the C-Cl bond in TBC,[55] to aid the generation of $[Al_2Cl_7]^-$, which subsequently forms $AlCl_3$ and also to activate C-H and C-C bonds for efficient hydride transfer and β-scission, respectively, during the cracking cycle.[58]

Various polyolefin plastics were tested, including polypropylene (PP) recovered from discarded surgical masks and commercial grades of low-density polyethylene (LDPE), linear low-density polyethylene (LLDPE), and high-density polyethylene (HDPE). Initial tests employed isopentane (iC_5) as an alkylating agent for olefinic scission products to thermodynamically favour the reaction by coupling the endothermic C-C bond cleavage with exothermic alkylation of olefins.[8,9] Using iC_5 as a sacrificial reactant poses challenges in terms of the origin and selectivity of the products. We later show that using DPC, can help us avoid using iC_5 altogether and still maintain high activity. In the initial tests, standard reaction mixture contained one of the above-mentioned polyolefins (0.2 g), dichloromethane (DCM ,3 mL) as a solvent (recoverable), iC_5 (1.29 mL), TBC as initiator (32.4 µl), DPC (30 mg) and Al_2Cl_6. After degassing under vacuum, the mixture was irradiated under visible light (400-1600 nm, 1.6 W cm^{-2}). We first optimised the amount of Al_2Cl_6 for PP conversion and found that 0.3 mmol (79.4 mg) was optimal, achieving quantitative conversion of 0.2 g of PP within 6 hours (Fig. S4). Using these optimized conditions, the upcycling of different polyolefins was evaluated with and without DPC under light irradiation (Fig. 2).

The presence of DPC significantly enhanced the conversion rate, nearly doubling the yield after 6 h compared to reactions without DPC (Fig. 2a-d). The kinetics was also found to be faster in the case when DPC was present, where most of the conversion occurred in the first 5 min of light irradiation. Furthermore, selectivity trends analysed after 6 h irradiation showed DPC-driven reactions favored the formation of lower alkanes (C_n, n<8, Fig. 2), attributed to more efficient carbenium ion generation and sequential C-C bond cleavage of higher chain hydrocarbons. As isopentane was used as the alkylating agent, the cumulative mass of final products was approximately double the initial polymer mass due to iC_5 incorporation (Fig. S5), posing challenges in selectivity and yield calculations. The liquid products were extracted and analysed using gas chromatography-mass spectrometry (GC-MS). The product distribution (after subtracting C_5 incorporation) was found to be mostly consisting of branched C_6-C_{10} alkanes (~85% for LDPE) (Fig. 2 e-h, S6-7). Gas-phase analysis detected only trace propane (<0.1 wt.%) and no methane or ethane (Fig. S8-9), indicating that the C-C bond cleavage predominantly proceeds through β-scission of carbenium ions rather than direct cracking of terminal carbon.

To probe the roles of iC_5 and TBC, control reactions were conducted for LDPE conversion by sequentially eliminating each component (Fig. 3a). After 15 min irradiation, significant decreases in conversion were observed when either iC_5 or TBC was excluded, with near-negligible conversion in the absence of both. This demonstrated that while DPC facilitated carbenium ion formation in the presence of TBC and $AlCl_3$, it does not serve as an independent active site.

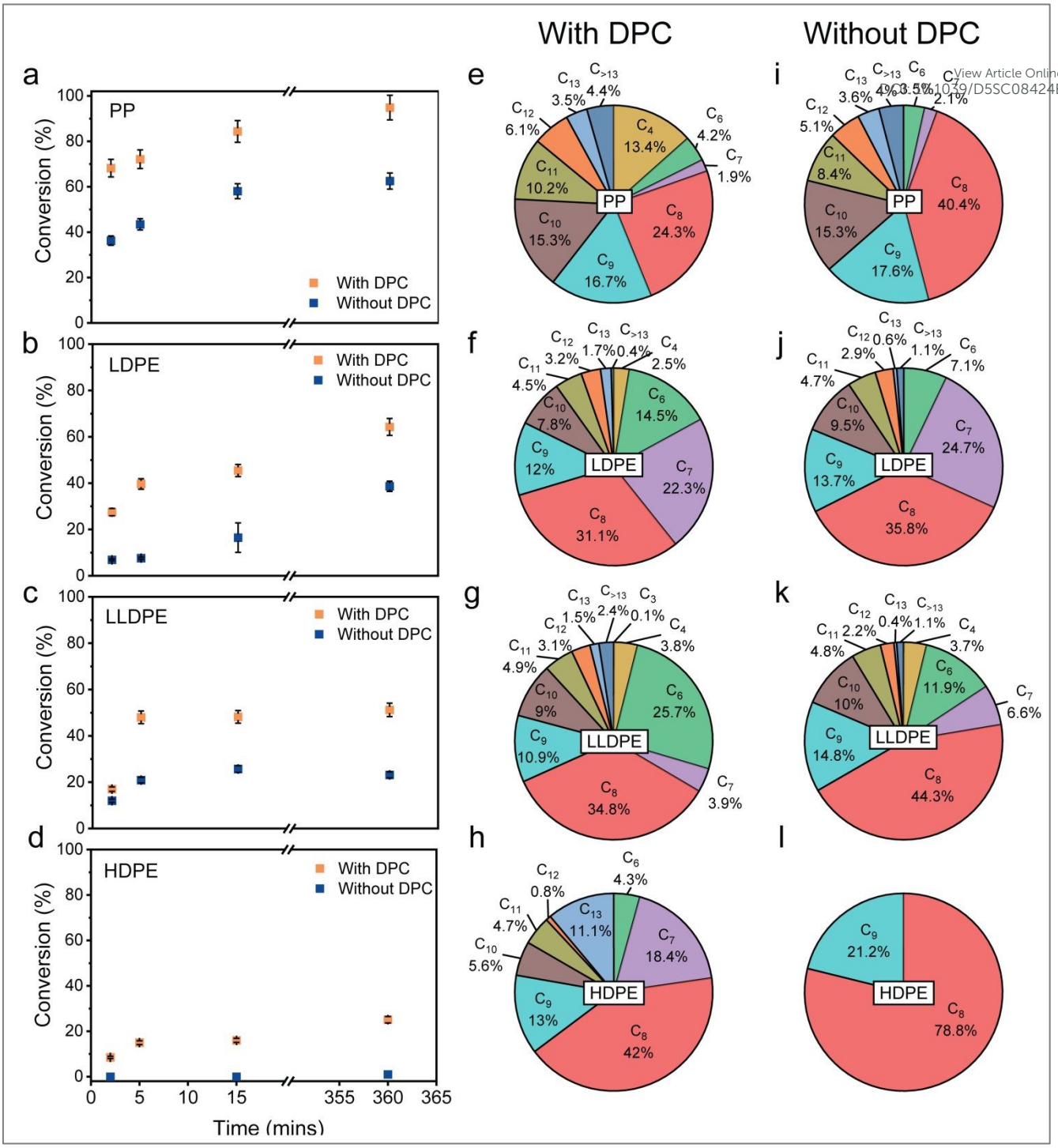

Fig. 2. One-pot catalytic upcycling of different types of plastics into liquid alkanes. Time-dependent conversion profile of **(a)** PP, **(b)** LDPE, **(c)** LLDPE and **(d)** HDPE in the presence of an alkylating reactant (iC_5) and the corresponding product distribution (excluding C_5) of tandem cracking-alkylation of different plastics waste with **(e-h)** *and* without DPC **(i-l)**. Reaction conditions: 0.2 g PE/PP, 3 mL DCM, 1.29 mL iC_5, 0.3 mmol Al_2Cl_6, 1.0 equivalent TBC, 30 mg DPC, under light of ~1.6 W cm^{-2} (400-1600 nm).

Further experiments were conducted, prolonging the light irradiation time to examine if isopentane could be eliminated altogether. In the absence of iC_5 and DPC, conversions remained low even after 24 h (Fig. 3b). However, in the presence of DPC, conversion significantly increased with time, confirming DPC's role in sustaining the reaction even without the iC_5 alkylating agent (Fig. 3b). Extending the reaction to 48 h with higher amount of DPC helped in achieving similar conversion levels as with iC_5. This highlights the intrinsic promotional role of DPC in facilitating plastic upcycling, even in the absence of the exothermic alkylation pathway. Notably, in the absence of iC_5, a substantial formation of lower alkanes (C_4-C_5) was observed, along with a notable increase in the production of C_8-C_9 cyclic hydrocarbons (~28.6%) (Fig. 3c). In contrast, the presence of iC_5 significantly suppressed

cyclization, maintaining cyclic product selectivity below 5% due to the preferential alkylation pathway (Fig. S10).

To enhance the conversion even further without using iC_5, the initial amount of LDPE was reduced to minimise competing reactive sites, leading to a substantial increase in conversion from approximately 45% to 85% (Fig. 3d, S11). Additionally, thermocatalytic reactions conducted at 70 °C (the typical post-illumination temperature measured *in-situ*, Fig. S12-13) in the dark showed that light irradiation remains crucial as the conversion rates with DPC in the dark were nearly half of those under illumination (Fig. 3d). This highlights a significant contribution of plasmonic non-thermal effects (electric field enhancement and hot electron injection) in DPC along with photothermal enhancement in facilitating TBC activation to generate carbenium ion and successive chain scission as discussed in later sections.

View Article Online
DOI: 10.1039/D5SC08424E

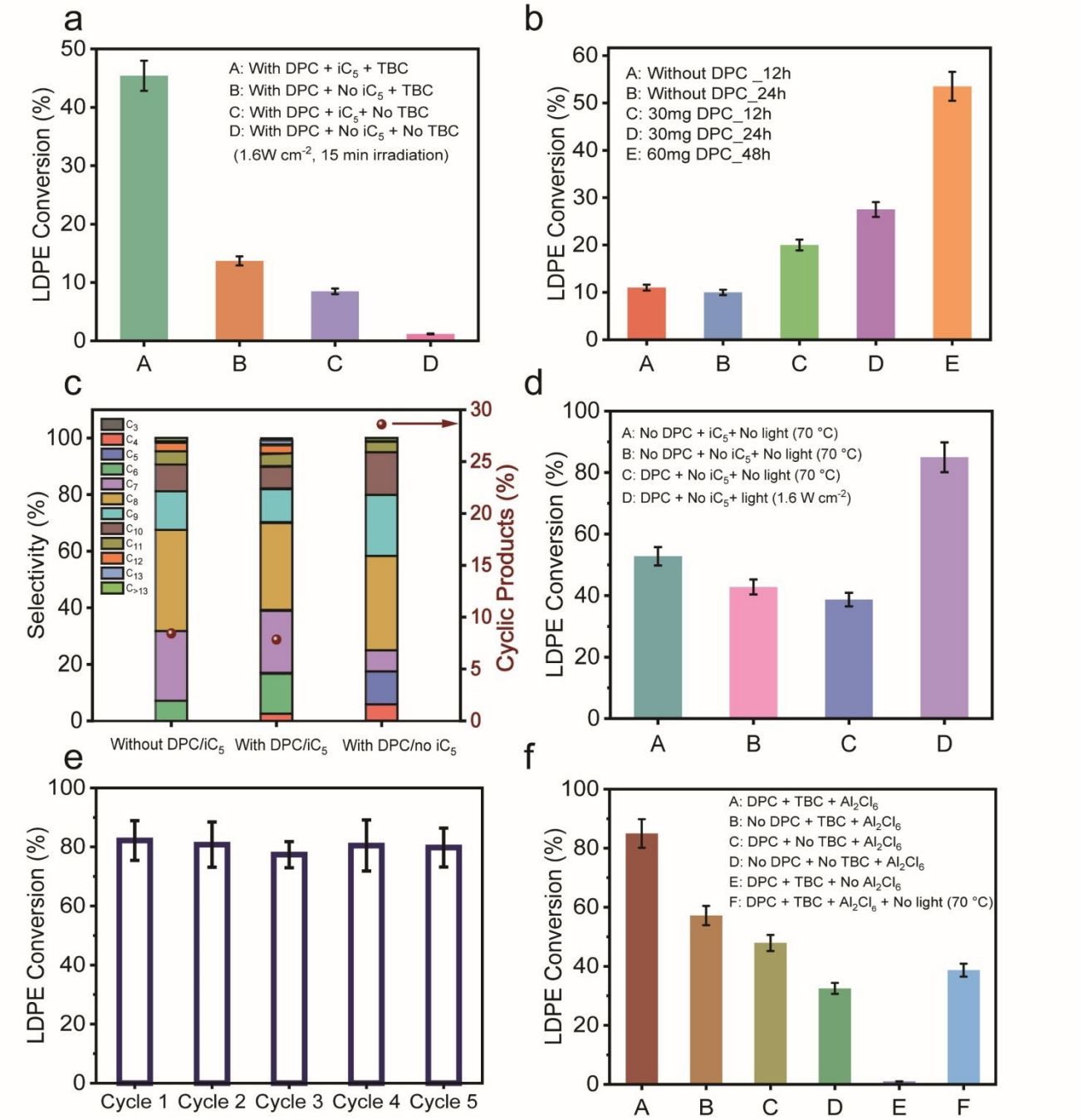

Fig. 3. Plasmonic conversion of LDPE without alkylating reactant (iC_5). (a) Various control experiments showing role of iC_5 and TBC; **(b)** LDPE conversion in the absence and presence of DPC and without iC_5 under prolonged light irradiation; **(c)** Comparison of product distribution of alkanes in the presence and absence of iC_5 after 6h; **(d)** Comparison of LDPE conversion under thermal conditions (70 °C) and under photocatalytic conditions; **(e)** Recycling test of DPC in LDPE upcycling using the DPC/Al_2Cl_6/TBC system; **(f)** Control experiments showing role of different components, DPC, Al_2Cl_6, TBC and light, after 60 min illumination. Reaction Conditions: LDPE (0.2g for a-c and 0.1g for d-f), 3 mL DCM, 0.3 mmol Al_2Cl_6, 1.0 equivalent TBC, 30 mg DPC, under light, ~1.6 W cm^{-2} (400-1600 nm).

DPC demonstrated excellent reusability over five cycles with minimal loss of activity, retained morphology and minimal sintering (Fig. 3e, S14-15, Table S1), emphasizing its potential in sustainable plastic upcycling. Moreover, component-specific control experiments highlighted the necessity of each system component, i.e. DPC, TBC, and Al_2Cl_6, for optimal conversion efficiency (Fig. 3f). These results confirm the synergistic roles of plasmonic activation mechanisms and Lewis acid catalysis in orchestrating effective solar-driven upcycling of plastic waste.

Uncovering the Mechanism Behind Plasmon-Driven LDPE Conversion. Following the systematic evaluation of the individual roles of DPC, TBC, and Al_2Cl_6 in facilitating the efficient conversion of LDPE, we propose a mechanistic pathway to elucidate their contributions to the upcycling process (Fig. 4a). The $AlCl_3$ Lewis acid is generated *in-situ* via the interaction of Al_2Cl_6 with TBC, producing $[Al_2Cl_7]^-$ and a tert-butyl carbenium ion, which initiates polymer cracking through hydride abstraction from the LDPE backbone (Fig. 4a). Lewis acidic $AlCl_3$ promotes heterolytic C–Cl cleavage by polarizing the C–Cl bond, stabilizing the released Cl^- as $AlCl_4^-/Al_2Cl_7^-$, as confirmed by ^{27}Al NMR (Fig. 4d–e, Fig. S16-19). This interpretation is supported by in situ DRIFTS, where the C–Cl stretching band (~800 cm^{-1}) exhibits a blue shift and reduced intensity, indicating progressive bond activation (Fig. S20). The resultant carbenium ion generated from TBC subsequently abstracts a hydride from the polyolefin backbone, thereby initiating chain cracking. Consistent with this pathway, the ^1H NMR spectra exhibit a signal at ~2.27 ppm, which can be assigned to the tertiary C–H proton of isobutane,[59] a key intermediate formed during hydride abstraction. Notably, this signal is most intense for the DPC system (Fig. S21), reflecting its more favorable reaction kinetics.

The plasmonic black gold catalyst enhances these steps through local field effects, hot-electron transfer, and photothermal heating,[53,55,60,61] facilitating carbenium ion formation. Although plasmonic excitation may transiently generate radical species due to hot electron transfer, rapid charge relaxation to maintain Au neutrality renders a sustained radical pathway unlikely.

Upon initiation, the polyolefin chains form primary carbenium ions via hydride transfer, catalyzed by $AlCl_3$,[8,9,58] which are energetically unfavorable. These unstable intermediates undergo successive rearrangements, specifically hydride and methyl shifts, to yield more stable tertiary carbenium ions. These then undergo type-A β-scission, resulting in the formation of an olefin and a shorter carbenium ion.[62] The resulting olefins can undergo either alkylation, in the presence of isopentane, to yield branched alkanes, or cyclization in its absence, thus driving the reaction forward (Fig. 4a, Fig. S10).

This mechanistic framework rationalizes the observed reactivity trend among various polyolefins. Polypropylene, characterized by methyl branches on alternating carbon atoms, facilitates the formation of tertiary carbenium ions and consequently exhibits the highest conversion. As the rate of β-scission increases with the branching degree, the trends observed for LDPE, LLDPE and HDPE could also be explained. Additionally, the more compact crystalline morphology of HDPE limits polymer-catalyst interactions, further reducing reactivity (Fig. 2).

To validate these mechanistic insights for polyolefin cleavage, we performed solid-state ^{13}C NMR analysis on post-reaction LDPE solids (Fig. 4b). A new peak at 20.4 ppm was observed, which was absent in the spectra of liquid-phase products. This peak has been previously assigned to β-methylene carbons adjacent to chain ends,[63,64] indicating chain cleavage. ^{13}C NMR peaks at 38.2, 34.6, 23.5, 14.9, 11.2 ppm corresponded to tertiary and secondary carbons in the branched side chains and terminal methyl groups, while peaks at 33.1, 27.7 ppm corresponded to methylene groups of the main backbone.[65,66] Interestingly, after the catalysis, the peak at 33.1 ppm, representing crystalline methylene (-CH_2- backbone in LDPE), showed reduced relative intensity, suggesting depolymerization. Furthermore, the absence of methane and ethane in the gas phase indicates that cleavage proceeds predominantly via internal β-scission rather than terminal bond breaking. Importantly, the presence of DPCs plays a central role in this process by generating localized plasmonic 'hot spots' under visible light, which polarize and activate C-Cl, C-C and C-H bonds, facilitating the formation and propagation of carbenium ions. These reactive intermediates drive a sequence of hydride shifts, isomerization, and β-scission steps, efficiently breaking down polyolefin chains.

Having established a mechanistic framework involving carbenium ion formation, hydride transfer, and subsequent β-scission, we next sought to elucidate the role of *in-situ* generated $AlCl_3$ as a Lewis acid in promoting the reaction. To investigate the nature of the catalytically active aluminium species, solution-

state ^{27}Al NMR spectroscopy was conducted during the plasmonic reaction. This analysis enabled real-time monitoring of $[Al_2Cl_7]^-$ and $[AlCl_4]^-$ species under light irradiation, both in the presence and absence of DPC (Fig.4d-f, S16–S19). $AlCl_3$, the active Lewis acid species, is formed through chloride abstraction by Al_2Cl_6. When Al_2Cl_6 abstracts Cl^- from TBC, it produces $[Al_2Cl_7]^-$ which subsequently dissociates and yields $AlCl_3$ and $[AlCl_4]^-$ (Fig. 4c). While $[Al_2Cl_7]^-$ has long been regarded as catalytically active,[67] recent kinetic analyses by Zhang et al.[8] have shown that it is the transient $AlCl_3$ formed from its dissociation that directly mediates catalysis. The relative concentrations of $AlCl_3$ can be approximated from the ratio of $[Al_2Cl_7]^-$ to $[AlCl_4]^-$ peak areas, scaled by the equilibrium constant (K^{-1}) (Fig. 4c).

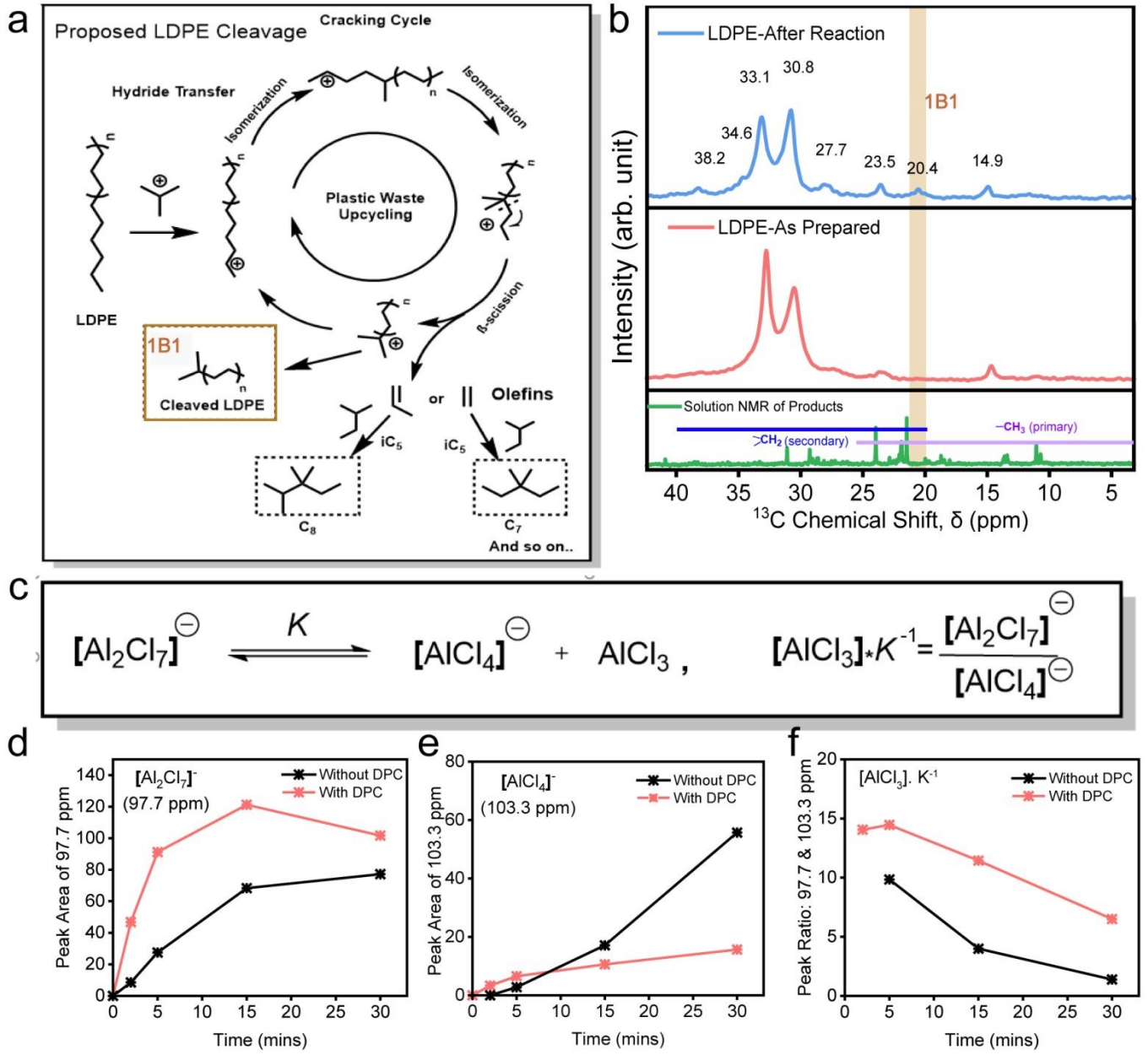

Fig. 4. Elucidating Reaction Mechanism. **(a)** Proposed LDPE cleavage in the plastic upcycling process; **(b)** ^{13}C Solid-state NMR spectra of solid LDPE particles before and after reaction for the identification of cleaved LDPE, along with solution NMR of products; **(c)** Schematic of the formation of active $AlCl_3$ species via dissociation of the dimeric $[Al_2Cl_7]^-$ (K - equilibrium constant). Monitoring Al species at different time intervals with/without DPC using solution state ^{27}Al NMR spectroscopy, peak area of **(d)** $[Al_2Cl_7]^-$ species, **(e)** $[AlCl_4]^-$ species and **(f)** their ratios at different light irradiation times.

Under light irradiation, the presence of DPC led to a consistently higher abundance of $[Al_2Cl_7]^-$ and a corresponding decrease in $[AlCl_4]^-$ compared to reactions conducted without DPC. This indicates that plasmonic effects in DPC (thermal and non-thermal) accelerate the generation of Cl^- ions by efficient cleavage of the C-Cl bond in TBC, thereby promoting rapid conversion of Al_2Cl_6 to $[Al_2Cl_7]^-$. In contrast, the

reaction without DPC exhibited a slower accumulation of $[Al_2Cl_7]^-$ (Fig. 4d) and a gradual increase in $[AlCl_4]^-$ over time (Fig. 4e), suggesting a competitive conversion pathway in which the delayed availability of Cl^- facilitates the formation of catalytically inactive $AlCl_4^-$. The net effect is a significantly higher concentration of $AlCl_3$ in the presence of DPC throughout the reaction, aligning closely with the enhanced LDPE conversion observed in the presence of DPC (Fig. 2,3). It should also be noted that the consequent decrease in $AlCl_3$ concentration could be due to the formation of an adduct with DCM, which could also play the role of carbenium ion initiator, in the presence of DPC, although moderately (Fig. S22).[68] These findings indicate that plasmonic DPC play a critical role by accelerating Cl^- generation and the formation of $[Al_2Cl_7]^-$ and thus $AlCl_3$, thereby promoting plasmonic enhanced Lewis acid-mediated hydride transfer and subsequent polymer chain scission.

Unraveling the Role of Plasmonic Black Gold in Sunlight-Driven LDPE Upcycling. To elucidate the contribution of hot electrons generated by plasmonic black gold, we systematically investigated the influence of photon flux on LDPE upcycling under visible light. Photocatalytic reactions were carried out under varying light intensities (Fig. 5a, S23). Initially, the reaction rate increased slowly with photon flux; however, at higher light intensities, the rate showed super-linear dependence, indicating multiple electron scattering events from DPC to adsorbed molecules.[69] At very high intensities, the rate plateaued, likely due to the saturation of available catalytic adsorption sites on the surface of the black gold.

In order to deconvolute thermal and non-thermal activations, experiments were performed under purely thermal conditions (in the dark) using external heating equivalent to the temperatures attained during light irradiation (Figs. 5b, S12-S13). In dark, LDPE conversion remained comparatively low (less than 40%), at respective temperatures. In contrast, the introduction of light irradiation significantly enhanced the reaction (more than 80%), leading to a higher conversion rate (Fig. 5b) indicating that the photothermal effects of plasmonic DPC alone were not sufficient for catalysis in this case. The Arrhenius analysis indicated the apparent activation energy to be 28 kJ/mol under light irradiation which was significantly lower as compared to 58 kJ/mol in dark conditions, again emphasizing the pivotal role of plasmonic non-thermal effects in facilitating polymer breakdown (Fig. 5c). A direct comparison over identical temperature ranges was not feasible because negligible conversion was observed in the dark at temperatures where measurable activity occurs under light irradiation. It should be also noted that the values of activation energies calculated are dramatically lower than the reported activation barriers (163–303 kJ/mol) for polyethylene depolymerization[70] owing to efficient Lewis acid catalysed polymer cracking.

To further elucidate the role of hot electrons in activating the C-Cl bond, we derived rate expressions via a quasi-equilibrium approximation and calculated the reaction orders (α_{RCl}) across varying concentrations of tert-butyl chloride (RCl) (Fig. 5d,e, S24).[60] Under the assumption that C-Cl bond scission is the rate-determining step (RDS). Fig. S24 shows how the reaction orders vary with respect to the reactant molecule, that is, the key for making $[Al_2Cl_7]^-$ and hence, reactive species $AlCl_3$. By assuming that surface coverage of adsorbate i, θ_i^* remains constant, the observed increase (Fig. 5f) in α_{RCl} (n = 0.43) can be ascribed to the dissociative adsorption of RCl being the RDS under photocatalytic conditions.[60] However, polyolefin cleavage also involves more complex, multi-step pathways beyond dissociative adsorption, including hydride/methyl shifts, carbocation rearrangements, isomerization and β-scission. Thus, the observed kinetics likely reflect a combination of interrelated elementary steps. Under visible-light photolysis, the generation of hot electrons by plasmonic excitation facilitates electron transfer to the σ*-orbital of the C-Cl bond in RCl, promoting its dissociative adsorption on the catalyst surface. This electronic pathway enhances C-Cl bond cleavage, thereby reducing the surface coverage of intact RCl species (θ_{RCl}*) and increasing the reactivity parameter α_{RCl} in the presence of light. Such electron transfer can also potentially help in activating the C-H and C-C bonds for the subsequent complex steps. These findings highlight the pivotal role of plasmonic catalysis in accelerating the reaction through electronic pathways that facilitate the dissociative adsorption of RCl, consequently leading to an increased formation of $[Al_2Cl_7]^-$ under photocatalytic conditions with plasmonic DPC, as confirmed by ^{27}Al NMR.

To directly probe the involvement of hot electrons, benzoquinone, an established electron scavenger,[49] was introduced in varying concentrations during the photocatalytic reaction (Fig. 5f). A progressive decline in LDPE conversion was observed with increasing

quencher concentration, highlighting that the suppression of hot electron availability adversely affects catalytic performance. This result indicates the significant involvement of hot electrons in driving key elementary steps of the depolymerization mechanism along with the photothermal activation.

View Article Online
DOI: 10.1039/D5SC08424E

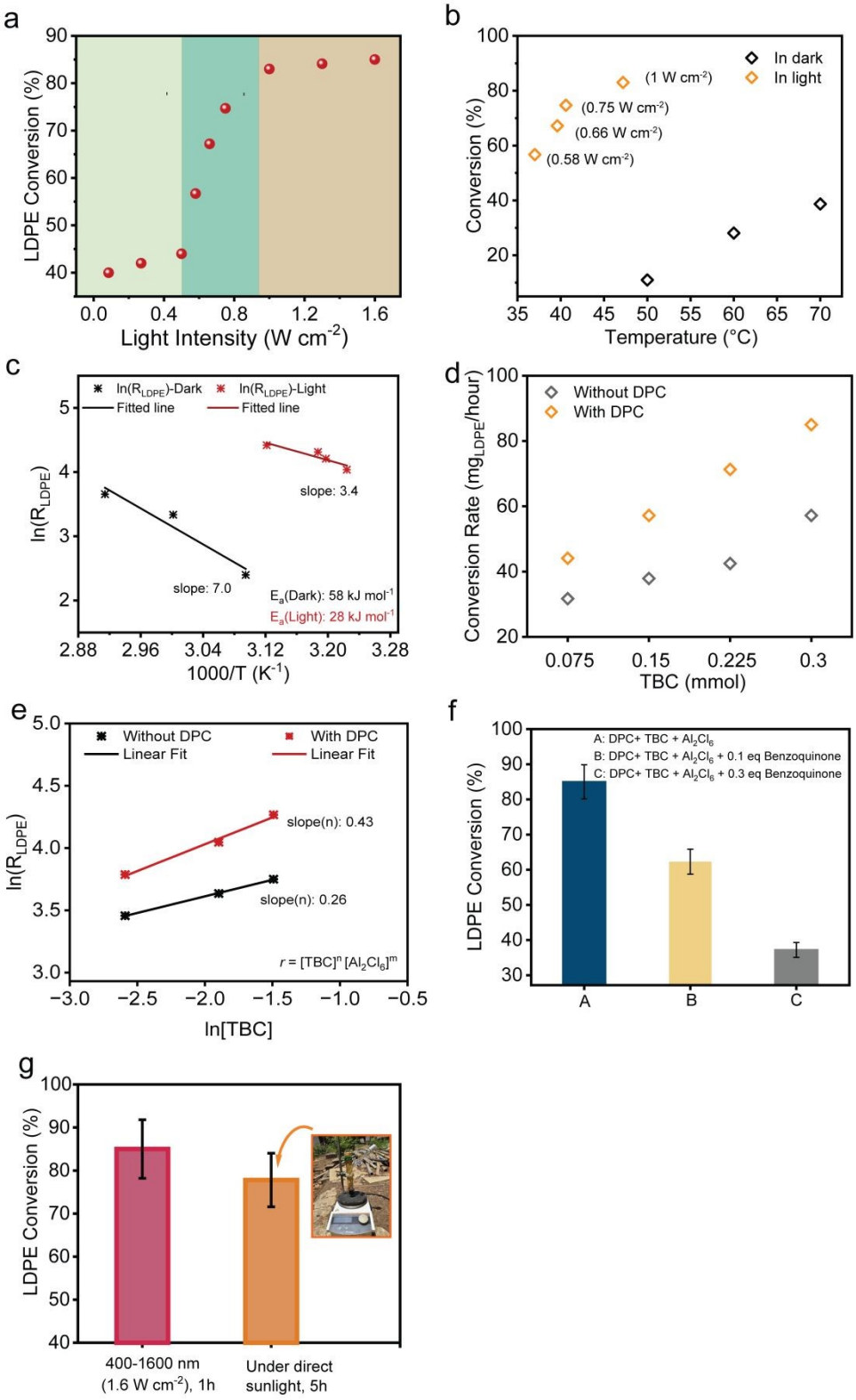

Fig. 5. Role of DPC in plasmonic conversion of LDPE. (a) LDPE conversion rate plotted as a function of light intensity; **(b)** LDPE conversion profile at different temperatures (in dark) as well as under light at different intensities; **(c)** Arrhenius plot for activation energies (E_a) of the plastic upcycling in the dark and light; **(d)** LDPE conversion with respect to TBC amount, **(e)** Determination of reaction order as a function TBC amount, with and without DPC under light irradiation (400 -1600 nm, 1.6 W cm^{-2}); **(f)** LDPE conversion rate after the addition of electron quencher benzoquinone in photocatalytic reaction; **(g)** Plasmonic plastic waste upcycling using direct sunlight. Reaction Conditions: 0.1g LDPE, 3 mL DCM, 0.3 mmol Al_2Cl_6, 1.0 equivalent TBC, 30 mg DPC, under light, ~1.6 W cm^{-2} (400-1600 nm), reaction time: 60 min

Outdoor Demonstration of Plasmonic LDPE Upcycling under Natural Sunlight. To evaluate the practical applicability and scalability of this approach, we conducted a small-scale outdoor demonstration using natural sunlight as the energy source (Fig. 5g). 0.1 gram of LDPE particles, 0.3 mmol of Al_2Cl_6, 3 ml of DCM, 32.4 µl TBC and 30 mg of DPC were loaded in a reactor. The reactor was directly exposed to natural sunlight, with the incident light intensity periodically recorded between 0.8 and 1 sun, resulting in a maximum reactor temperature of approximately 45 °C (Fig. S25). Remarkably, after 5 h of reaction, LDPE conversion comparable to that achieved under laboratory conditions (16 sun, 1 h) was obtained (Fig. 5g). This efficient performance highlights the practicality of the system, which operates without the need for solar concentrators or external heating infrastructure.

CONCLUSIONS

We have demonstrated a sunlight-only strategy for the catalytic upcycling of plastic waste into value-added hydrocarbons using plasmonic black gold. Under visible-to-NIR irradiation at ambient temperature, our system achieves LDPE conversions exceeding 80 % within one hour and yields predominantly C_6–C_{10} branched alkanes with >85 % selectivity, without external heating, sacrificial reagents, or ionic liquids. Comparative thermal controls, activation energy analysis, and electron scavenging studies, all indicate significant contributions from hot electron-mediated efficient C-Cl cleavage using plasmonic black gold along with photothermal effects.

Quasi-equilibrium microkinetic analysis revealed that plasmonic effects under illumination helped the dissociative adsorption of tert-butyl chloride (RCl), as evidenced by an increase in reaction order. Hot electrons non-thermally excite and cleave the C-Cl bond, lowering θ_{RCl}* and helping in the formation of $[Al_2Cl_7]^-$ and hence, more active Lewis-acid $AlCl_3$ species. ^{27}Al NMR analysis of the reaction mixture at different time intervals revealed that plasmonic effects in DPC promote the formation of catalytically active $AlCl_3$ species, which directly correlates with the observed upcycling rate.

The catalyst remained robust over at least five consecutive cycles, and a proof-of-concept outdoor experiment under one-sun illumination confirmed the practical feasibility of this plasmonic upcycling depicted in this work without solar concentrators or external heaters.

View Article Online
DOI: 10.1039/D5SC08424E

This work represents the first example of plasmon-enabled plastic upcycling powered exclusively by sunlight, merging broadband light harvesting, hot-carrier chemistry, and Lewis acid catalysis into a single, sustainable platform. By eliminating the need for high-temperature reactors, toxic solvents, or hydrogen donors, this approach opens new avenues for low-carbon, on-site conversion of plastic waste into chemical feedstocks and fuels.

Data availability

The data that support the findings of this work are available within the article and its supplementary information files.

Acknowledgements

We acknowledge the funding support of the Department of Atomic Energy 12-R&D-TFR-RTI4003. We acknowledge the EM and XRD facility of TIFR, Mumbai. We acknowledge Prof. Vipin Agarwal for the solid-state NMR experiment at TIFR, Hyderabad. We thank Mr. Rishi Verma from TIFR, Mumbai, for the in-depth discussion. We acknowledge the support of the central workshop facility of TIFR, Mumbai.

Author contributions

V.P. proposed the research direction, designed the project, and guided the project. S.S and V.P. designed various experiments. S.S performed the experiments (synthesis, characterizations, catalysis), assisted by G.S. M.J. assisted with the solution state NMR studies. Data was analyzed by S.S., G.S., and V.P. The overall manuscript was written by G.S., S.S. and V.P.. Everyone commented on the manuscript.

Competing interests

The authors declare no competing interests.

Data and materials availability: All data needed to evaluate the conclusions in the paper are present in the paper and/or the Supplementary Materials.

Supplementary Materials: Supplementary information (Experimental details, Figures S1 to S25, and Tables S1) is available for this paper.

Correspondence should be addressed to V.P. (vivekpol@tifr.res.in)

REFERENCES

1. Van Geem, K. M. Plastic Waste Recycling Is Gaining Momentum. *Science* **2023**, *381*, 60-608.
2. Stegmann, P.; Daioglou, V.; Londo, M.; van Vuuren, D. P.; Junginger, M. Plastic Futures and Their CO_2 Emissions. *Nature* **2022**, *612*, 272-276.
3. Garcia, J. M.; Robertson, M. L. The Future of Plastics Recycling. *Science* **2017**, *358*, 870–872.
4. Tang, Z.; Xiao, G.; Wang, Z.; Zhao, Y.; Su, H. Chemical Recycling and Upcycling of Waste Plastics: A Review. *Green Chem. Technol.* **2024**, *1* , 10003.
5. Du, J.; Zeng, L.; Yan, T.; Wang, C.; Wang, M.; Luo, L.; Wu, W.; Peng, Z.; Li, H.; Zeng, J. Efficient Solvent- and Hydrogen-Free Upcycling of High-Density Polyethylene into Separable Cyclic Hydrocarbons. *Nat. Nanotechnol.* **2023**, *18*, 772-779.
6. Sun, S.; Huang, W. Chemical Upcycling of Polyolefin Plastics Using Structurally Well-Defined Catalysts. *JACS Au* **2024**, 4, 2081-2098.
7. Zhang, M.; Zhang, Y.; Li, Y.; Wang, Y.; Wang, Z.; Wang, X. Catalytic Strategies for Upvaluing Plastic Wastes. *Chem* **2022**, *8*, 3145-3166.
8. Zhang, W.; Kim, S.; Wahl, L.; Khare, R.; Hale, L. V.; Hu, J.; Camaioni, D. M.; Gutiérrez, O. Y.; Liu, Y.; Lercher, J. A. Low-Temperature Upcycling of Polyolefins into Liquid Alkanes via Tandem Cracking-Alkylation. *Science* **2023**, *379*, 807-811.
9. Zhang, W.; Yang, B.; Jackson, B. A.; Zhao, J.; Shi, H.; Camaioni, D. M.; Kim, S.; Wang, H.; Szanyi, J.; Lee, M.-S.; Chen, J. G.; Lercher, J. A. Integrated Low-Temperature PVC and Polyolefin Upgrading. *Science* **2025**, 390, 88-94.
10. Ran, J.; Talebian-Kiakalaieh, A.; Zhang, S.; Hashem, E. M.; Guo, M.; Qiao, S.-Z. Recent Advancement on Photocatalytic Plastic Upcycling. *Chem. Sci.* **2024**, *15*, 1611-1637.
11. Wimberger, L.; Ng, G.; Boyer, C. Light-Driven Polymer Recycling to Monomers and Small Molecules. *Nat. Commun.* **2024**, *15*, 2510.
12. Zhang, X.; Zu, W.; Lee, L. Y. S. Crucial Role of Pre-Treatment in Plastic Photoreforming for Precision Upcycling. *npj Mater. Sustain.* **2025**, *3*, 3.
13. Deng, Y.; Chen, J.; Zhang, Q.; Cao, M. Photocatalytic Upcycling of Different Types of Plastic Wastes: A Mini Review. *ChemPlusChem* **2024**, *89*, e202400336.
14. Lee, W. H.; Park, H.; Lee, C. W.; Kim, H.; Jeong, J. H.; Yun, J. I.; Bang, S.-U.; Heo, J.; Ahn, K. H.; Cha, G. D.; Bootharaju, M. S.; Lee, B.-H.; Ryu, J.; Kim, M.; Hyeon, T.; Kim, D.-H. Polymeric Stabilization at the Gas–Liquid Interface for Durable Solar Hydrogen Production from Plastic Waste. *Nat. Nanotechnol.* **2025**, 20, 1237-1246.
15. Kang, H.; Washington, A.; Capobianco, M. D.; Yan, X.; Cruz, V. V.; Li, Y.; Li, Y.; Zhang, Y.; Wu, J.; Xu, Y.; Zhao, Y. Concentration-Dependent Photocatalytic Upcycling of Poly(ethylene terephthalate) Plastic Waste. *ACS Mater. Lett.* **2023**, *5*, 3032-3041.
16. Uekert, T.; Kasap, H.; Reisner, E. Photoreforming of Nonrecyclable Plastic Waste over a Carbon Nitride/Nickel Phosphide Catalyst. *J. Am. Chem. Soc.* **2019**, 141, 15201-15210.
17. Jiao, X.; Zheng, K.; Chen, Q.; Li, X.; Li, Y.; Shao, W.; Xu, J.; Zhu, J.; Pan, Y.; Sun, Y.; Xie, Y. Photocatalytic Conversion of Waste Plastics into C_2 Fuels under Simulated Natural Environment Conditions. *Angew. Chem. Int. Ed.* **2020**, *59*, 15497-15501.
18. Li, C.; Kong, X. Y.; Lyu, M.; Tay, X. T.; Đokić, M.; Chin, K. F.; Yang, C. T.; Lee, E. K. X.; Zhang, J.; Tham, C. Y.; Chan, W. X.; Lee, W. J.; Lim, T. T.; Goto, A.; Sullivan, M. B.; Soo, H. S. Upcycling of Non-Biodegradable Plastics by Base Metal Photocatalysis. *Chem* **2023**, *9*, 2683-2700.
19. Mountanea, O. G.; Skolia, E.; Kokotos, C. G. Photochemical Aerobic Upcycling of Polystyrene Plastics via Synergistic Indirect HAT Catalysis. *Chem. Eur. J.* **2024**, *30*, e202401588.
20. Nikitas, N. F.; Skolia, E.; Gkizis, P. L.; Triandafillidi, I.; Kokotos, C. G**.** Photochemical Aerobic Upcycling of Polystyrene Plastics to Commodity Chemicals Using Anthraquinone as the Photocatalyst. *Green Chem.* **2023**, *25*, 4750-4759.
21. Zhang, S.; Wang, J.; Su, D.; Xiao, X. Facile Visible-Light Upcycling of Diverse Waste Plastics Using a Single Organocatalyst with Minimal Loadings. *Nat. Commun.* **2025**, *16*, 4188.
22. Uekert, T.; Kuehnel, M. F.; Wakerley, D. W.; Reisner, E. Plastic Waste as a Feedstock for Solar-Driven H_2 Generation. *Energy Environ. Sci.* **2018**, *11*, 2853-2857.
23. Wu, Y.; Nguyen, P. T. T.; Wong, S. S.; Feng, M.; Han, P.; Yao, B.; He, Q.; Sum, T. C.; Zhang, T.; Yan, N. Photocatalytic Upcycling of Polylactic Acid to Alanine by Sulfur Vacancy-Rich Cadmium Sulfide. *Nat. Commun.* **2025**, *16*, 846.
24. Xu, J.; Jiao, X.; Zheng, K.; Shao, W.; Zhu, S.; Li, X.; Zhu, J.; Pan, Y.; Sun, Y.; Xie, Y. Plastics-to-Syngas Photocatalysed by Co–Ga_2O_3 Nanosheets. *National Science Review* **2022**, *9*, nwac011.
25. Jiao, X.; Hu, Z.; Zheng, K.; Zhu, J.; Wu, Y.; Zhang, X.; Hu, J.; Yan, W.; Zhu, J.; Sun, Y.; Xie, Y. Direct Polyethylene Photoreforming into Exclusive Liquid Fuel over Charge-Asymmetrical Dual Sites under Mild Conditions. *Nano Lett.* **2022**, *22* , 10066-10072.
26. Zhang, W.; Chen, Z.; Jiang, Y.-X.; Liao, L.-L.; Wang, W.; Ye, J.-H.; Yu, D.-G. Arylcarboxylation of Unactivated Alkenes with CO_2 via Visible-Light Photoredox Catalysis. *Nat. Commun.* **2023**, *14*, 3529.
27. Bhattacharjee, S.; Guo, C.; Lam, E.; Holstein, J. M.; Rangel Pereira, M.; Pichler, C. M.; Pornrungroj, C.; Rahaman, M.; Uekert, T.; Hollfelder, F.; Reisner, E. Chemoenzymatic Photoreforming: A Sustainable Approach for Solar Fuel Generation from Plastic Feedstocks. *J. Am. Chem. Soc.* **2023**, *145*, 20355-20364.
28. Liu, Y.; Wang, X.; Li, X.; Ye, Z.; Sham, T.-K.; Xu, P.; Cao, M.; Zhang, Q.; Yin, Y.; Chen, J**.** Universal and Scalable Synthesis of Photochromic Single-Atom Catalysts for Plastic Recycling. *Nat. Commun.* **2024**, *15*, 9357.
29. Xu, Zhen; Pan, Fuping; Sun, Mengqi; Xu, Jianjun; Munyaneza, Nuwayo Eric; Croft, Zacary L.; Cai, Gangshu (George); Liu, Guoliang. Cascade Degradation and Upcycling of Polystyrene Waste to High-Value Chemicals. *Proc. Natl. Acad. Sci. U.S.A.* **2022**, *119*, e2203346119.
30. Huang, Z.; Shanmugam, M.; Liu, Z.; Brookfield, A.; Bennett, E. L.; Guan, R.; Vega Herrera, D. E.; Lopez-Sanchez, J. A.; Slater, A. G.; McInnes, E. J. L.; Qi, X.; Xiao, J. Chemical Recycling of Polystyrene to Valuable Chemicals via Selective Acid-Catalyzed Aerobic Oxidation under Visible Light. *J. Am. Chem. Soc.* **2022**, *144*, 6532-6542.
31. Oh, S.; Stache, E. E. Chemical Upcycling of Commercial Polystyrene via Catalyst-Controlled Photooxidation. *J. Am. Chem. Soc.* **2022**, *144*, 5745-5749.
32. Luo, H.; Yao, D.; Zeng, K.; Li, J.; Yan, S.; Zhong, D.; Hu, J.; Yang, H.; Chen, H. Solar Pyrolysis of Waste Plastics with

Photothermal Catalysts for High-Value Products. *Fuel Processing Technology* **2022**, *230*, 107205.

33. Miao, Y.; Zhao, Y.; Waterhouse, G. I. N.; Shi, R.; Wu, L.-Z.; Zhang, T. Photothermal Recycling of Waste Polyolefin Plastics into Liquid Fuels with High Selectivity under Solvent-Free Conditions. *Nat. Commun.* **2023**, *14*, 4242.
34. Liu, Y.; Zhang, C.; Feng, J.; Wang, X.; Ding, Z.; He, L.; Zhang, Q.; Chen, J.; Yin, Y. Integrated Photochromic-Photothermal Processes for Catalytic Plastic Upcycling. *Angew. Chem. Int. Ed.* **2023**, *135*, e202308930.
35. Kugelmass, L. H.; Tagnon, C.; Stache, E. E. Photothermal Mediated Chemical Recycling to Monomers via Carbon Quantum Dots. *J. Am. Chem. Soc.* **2023**, *145*, 16090-16097.
36. Xing, C.; Mao, C.; Wang, S.; Zhou, Y.; Wu, L.; Zhang, D.; Kang, D.; Yang, D.; Gong, W.; Wei, W.; Wang, L.; Li, C.; Ozin, G. A.; Yang, D.; Sun, W. Ambient Solar Thermal Catalysis for Polyolefin Upcycling Using Copper Encapsulated in Silicon Nanosheets and Chloroaluminate Ionic Liquid. *Nat Catal* **2025**, *8*, 556-568.
37. Hu, C.; Dong, Y.; Shi, Q.; Long, R.; Xiong, Y. Catalysis under Electric-/Magnetic-/Electromagnetic-Field Coupling. *Chem. Soc. Rev.* **2025**, *54*, 524-559.
38. Aslam, U., Rao; V. G., Chavez, S.; Linic, S. Catalytic Conversion of Solar to Chemical Energy on Plasmonic Metal Nanostructures. *Nat. Catal.* **2018**, *1*, 656-665.
39. Cortés, E.; Besteiro, L. V.; Alabastri, A.; Baldi, A.; Tagliabue, G.; Demetriadou, A.; Narang, P. Challenges in Plasmonic Catalysis. *ACS Nano* **2020**, *14*, 16202-16219.
40. Lee, H.; Park, Y.; Song, K.; Park, J. Y. Surface Plasmon-Induced Hot Carriers: Generation, Detection, and Applications. *Acc. Chem. Res.* **2022**, *55*, 3727-3737.
41. Verma, R.; Belgamwar, R.; Polshettiwar, V. Plasmonic Photocatalysis for CO_2 Conversion to Chemicals and Fuels. *ACS Materials Lett.* **2021**, *3*, 574-598.
42. Cortés, E.; Grzeschik, R.; Maier, S. A.; Schlücker, S. Experimental Characterization Techniques for Plasmon-Assisted Chemistry. *Nat Rev Chem* **2022**, *6*, 259-274.
43. Verma, R.; Sharma, G.; Polshettiwar, V. The Paradox of Thermal vs. Non-Thermal Effects in Plasmonic Photocatalysis. *Nat. Commun.* **2024**, *15*, 7974.
44. Stefancu, A.; Halas, N. J.; Nordlander, P.; Cortes, E. Electronic Excitations at the Plasmon–Molecule Interface. *Nat. Phy.* **2024**, *20*, 1065-1077.
45. Halas, N. J.; Lal, S.; Chang, W. -S.; Link, S.; Nordlander, P. Plasmons in Strongly Coupled Metallic Nanostructures. *Chem. Rev.* **2011**, *111*, 3913-3961.
46. Yu, S.; Jain, P.K. Plasmonic Photosynthesis of C_1–C_3 Hydrocarbons from Carbon Dioxide Assisted by an Ionic Liquid. *Nat. Commun.* **2019**, *10*, 2022.
47. Kim, Y.; Smith, J. G.; Jain, P. K. Harvesting Multiple Electron–Hole Pairs Generated Through Plasmonic Excitation of Au Nanoparticles. *Nature. Chem.* **2018**, *10*, 763-769.
48. Brongersma, M. L.; Halas, N. J.; Nordlander, P. Plasmon-Induced Hot Carrier Science and Technology. *Nat. Nanotech.* **2015**, *10*, 25-34
49. Singh, S.; Verma, R.; Kaul, N.; Sa, J.; Punjal, A.; Prabhu, S.; Polshettiwar, V. Surface Plasmon-Enhanced Photo-Driven CO_2 Hydrogenation by Hydroxy-Terminated Nickel Nitride Nanosheets. *Nat. Commun.* **2023**, *14*, 2551.
50. Belgamwar, R.; Singhvi, C.; Sharma, G.; Paidi, V. K.; Glatzel, P.; Yamazoe, S.; Sarawade, P.; Polshettiwar, V. Synthesis of Synergistic Catalysts: Integrating Defects, SMSI, and Plasmonic Effects for Enhanced Photocatalytic CO_2 Reduction. *Chem. Sci.* **2025**, *16*, 9766-9784
51. Dhiman, M.; Maity, A.; Das, A.; Belgamwar, R.; Chalke, B.; Lee, Y.; Sim, K.; Nam, J. –M.; Polshettiwar, V. Plasmonic Colloidosomes of Black Gold for Solar Energy Harvesting and Hotspots Directed Catalysis for CO_2 to Fuel Conversion. *Chem. Sci.* **2019**, *10*, 6594-6603.
52. Verma, R.; Kundu, S.; Polshettiwar, V. One-pot Synthesized Plasmonic Black Gold Nanoparticles for Efficient Photocatalytic CO Oxidation. *J. Mater. Chem. A* **2024**, *12*, 27235-27245.
53. Sharma, G.; Polshettiwar, V. Black Gold for Broadband Solar Harvesting. *Nano Lett.* **2025**, 25, 16311-16322.
54. Verma, R.; Belgamwar, R.; Chatterjee, P.; Vadell, R. -B.; Sa, J.; Polshettiwar, V. Nickel Laden Dendritic Plasmonic Colloidosomes of Black Gold: Forced Plasmon Mediated Photocatalytic CO_2 Hydrogenation. *ACS Nano* **2023**, *17*, 4526-4538.
55. Verma, R.; Tyagi, R.; Voora, V. K.; Polshettiwar, V. Black Gold-Based "Antenna-Reactor" to Activate Non-Plasmonic Nickel: Photocatalytic Hydrodechlorination and Hydrogenation Reactions. *ACS Catal.* **2023**, *13*, 7395-7406.
56. Sharma, G.; Verma, R.; Masuda, S.; Badawy, K.; Singh, N.; Tsukuda, T.; Polshettiwar, V. Pt-Doped Ru Nanoparticles Loaded on 'Black Gold' Plasmonic Nanoreactors as Air Stable Reduction Catalysts. *Nat. Commun.* **2024**, *15*, 713.
57. Sharma, G.; Singhvi, C.; Mishra, G.; Nandi, A.; Schuck, G.; Grimm, N.; Wallacher, D.; Kumar, A.; Nukala, P.; Nath, S.; Ghosh, S.; Polshettiwar, V. Hot Electron–Driven Tandem CO_2 Reduction and Propane Dehydrogenation over Plasmonic Black Gold Nanoreactors. *Proc. Natl. Acad. Sci. U.S.A.* **2025**, 122, e2520317122.
58. Xue, N.; Vjunov, A.; Schallmoser, S.; Fulton, J. L.; Sanchez-Sanchez, M.; Hu, J. Z.; Mei, D.; Lercher, J. A. Hydrolysis of Zeolite Framework Aluminum and Its Impact on Acid Catalyzed Alkane Reactions. *J. Catal* **2018**, *365*, 359-366.
59. Schoofs, B.; Schuermans, J.; Schoonheydt, R. A. Hydrogen–Deuterium Exchange Reactions with Isobutane over Acid Zeolites. *Micro. Meso. Mater.* **2000**, 35–36, 99–111.
60. Robatjazi, H.; Bao, J. L.; Zhang, M.; Zhou, L.; Christopher, P.; Carter, E. A.; Nordlander, P.; Halas, N. J. Plasmon-Driven Carbon–Fluorine ($C(Sp^3)$–F) Bond Activation with Mechanistic Insights into Hot-Carrier-Mediated Pathways. *Nat Catal* **2020**, 3, 564-573.
61. Verma, P. K.; Nayak, S. K.; Bhardwaj, K.; Yamijala, S. S. R. K. C. Realizing Direct Hot-Electron Transfer from Metal Nanoparticles to Per- and Polyfluoroalkyl Substances. *J. Phys. Chem. Lett.* **2025**, 16, 4536-4546.
62. Sun, J.; Lee, Y.-H.; Yappert, R. D.; LaPointe, A. M.; Coates, G. W.; Peters, B.; Abu-Omar, M. M.; Scott, S. L. Bifunctional Tandem Catalytic Upcycling of Polyethylene to Surfactant-Range Alkylaromatics. *Chem.* **2023**, *9*, 2318–2336.
63. Liu, H; Zhao, W; Yu, J; Yang, W; Hao, X; Redshaw, C; Chen, L; Wen-Hua Sun, W. H. Synthesis, characterization and ethylenepolymerization behavior of nickel dihalide complexes bearing bulky unsymmetrical α-diimine ligands. *Catal. Sci. Technol.*, **2012**, *2*, 415-422.
64. Hansen, E. W.; Blom, R.; Bade, O. M. N.M.R. Characterization of Polyethylene with Emphasis on Internal Consistency of Peak

Intensities and Estimation of Uncertainties in Derived Branch Distribution Numbers. *Polymer* **1997**, *38* , 4295-4304.

65. Klein, P. G.; Driver, M. A. N. Chain Diffusion in Ultralong n-Alkane Crystals Studied by ^{13}C NMR. *Macromolecules* **2002**, *35*, 6598-6612.

66. Cholli, A. L.; Ritchey, W. M.; Koenig, J. L.; Veeman, V. S. Separation of Components in Crystalline and Amorphous Regions of Polyethylene by Solid-State ^{13}C NMR Spectroscopy. *Spectrosc. Lett.* **1988**, *21*, 519-531.

67. Kore, R.; Berton, P.; Kelley, S. P.; Aduri, P.; Katti, S. S.; Rogers, R. D. Group IIIA Halometallate Ionic Liquids: Speciation and Applications in Catalysis. *ACS Catal.* **2017**, *7*, 7014-7028.

68. Zhang, W.; Yao, H.; Khare, R.; Zhang, P.; Yang, B.; Hu, W.; Ray, D.; Hu, J.; Camaioni, D. M.; Wang, H.; Kim, S.; Lee, M.; Sarazen, M. L.; Chen, J. G.; Lercher, J. A. Chloride and Hydride Transfer as Keys to Catalytic Upcycling of Polyethylene into Liquid Alkanes. *Angew Chem Int Ed* **2024**, *63*, e202319580.

69. Christopher, P.; Xin, H.; Marimuthu, A.; Linic, S. Singular Characteristics and Unique Chemical Bond Activation Mechanisms of Photocatalytic Reactions on Plasmonic Nanostructures. *Nat. Mater* **2012**, *11*, 1044-1050.

70. Ellis, L. D.; Rorrer, N. A.; Sullivan, K. P.; Otto, M.; McGeehan, J. E.; Román-Leshkov, Y.; Wierckx, N.; Beckham, G. T. Chemical and Biological Catalysis for Plastics Deconstruction, Recycling, and Upcycling. *Nat. Catal.* **2021**, *4*, 539–556.

View Article Online
DOI: 10.1039/D5SC08424E

View Article Online
DOI: 10.1039/D5SC08424E

Data and materials availability: All data needed to evaluate the conclusions in the paper are present in the paper and/or the Supplementary Materials.